CIRP Annals - Manufacturing Technology 68 (2019) 229–232

Contents lists available at ScienceDirect

CIRP Annals - Manufacturing Technology

journal homepage: http://ees.elsevier.com/cirp/default.asp

# High-speed X-ray investigation of melt dynamics during continuous-wave laser remelting of selective laser melted Co-Cr alloy

Brodan Richter [a], Nena Blanke [b], Christian Werner [b], Niranjan D. Parab [c], Tao Sun [c], Frank Vollertsen (1)[b,d], Frank E. Pfefferkorn (2)[a,*]

[a] Department of Mechanical Engineering, University of Wisconsin-Madison, Madison, WI, 53706 USA
[b] Bremer Institut für angewandte Strahltechnik GmbH, Bremen, 28359, Germany
[c] X-ray Science Division, Advanced Photon Source, Argonne National Laboratory, Lemont, IL, 60439, USA
[d] University of Bremen, Bremen, 28359, Germany

ARTICLE INFO

*Article history:*
Available online 7 May 2019

*Keywords:*
Laser
Selective laser melting (SLM)
X-ray imaging

ABSTRACT

The objective of this study is to quantify the melt pool dynamics during continuous wave laser remelting of a Co-Cr alloy manufactured using selective laser melting. This knowledge will inform process improvement and numerical modeling of laser remelting. A high-intensity X-ray beam imaged a 2 mm × 0.5 mm area of the surface with a 50 kHz framerate. Analysis of these videos quantified the melt pool surface wave movement and compared this to the initial surface features. The results indicate that the keyhole and its characteristic oscillations can suppress large wavelength features on the initial surface.



## 1. Introduction

Additive manufacturing has seen tremendous growth due to the substantial benefits the process provides to part complexity and customizability. However, the surfaces of additively manufactured parts have high roughness that often necessitate some type of post-processing to produce usable surfaces [1]. One potential post-processing technique is laser remelting with the goal of smoothing, i.e., laser polishing. This process involves a secondary melt event on the surface of the post-built sample through laser irradiation in which surface asperities in the melt pool smooth out due to surface tension [2,3]. Due to the quick, selective, and contactless nature of the process, laser polishing holds promise as an ideal process for smoothing additive manufactured metallic parts.

Laser polishing has traditionally been performed in one of two primary modes: continuous wave, in which the laser remains continuously on, and pulsed, in which the laser pulses to create distinct melt and resolidification events [3]. In general, laser polishing through remelting has normally been assumed to remain in a conduction-heating mode, with no or little laser ablation. However, at higher fluxes the laser vaporizes material, causing recoil pressure, melt pool displacement, and the formation of a self-sustaining keyhole. In this work, laser polishing in continuous wave with a keyhole present is studied for the first time. There are numerous techniques that have been utilized to observe laser-based processing with a keyhole, such as acoustic measurements, infrared and visible light imaging, and X-ray imaging [4]. X-ray imaging provides the advantage of capturing the internal structure of the samples, e.g., cross-section of the melt pool. This allows for the observation of keyhole and keyhole-formed porosity [5]. Recently, high-speed X-ray imaging (HSXRI) at a rate of 50 kHz has been used to study powder consolidation in powder bed fusion processes [6]. The capture rate was further increased to 6.5 MHz, giving ultra-fast temporal resolution of the consolidation and keyhole dynamics [7].

The ultra-fast imaging of the keyhole also shows waves propagating along the internal surface of the keyhole. Prior work has explored the frequency of wave vibrations within the keyhole, reporting values in the kHz range [8]. That work also demonstrated that keyhole vibrations occur in both stable and unstable keyholes and that higher powers usually led to worse keyhole stability. Other work observing surface waves in laser keyhole welding using optical imaging estimated wave velocity and wave number as approximately 2 m/s and 20,944 respectively, which correlates to a vibrational frequency of approximately 6 kHz [9]. In this work, the cross-section of the melt pool during laser polishing by means of high-speed X-ray imaging is presented (Fig. 1). It also investigates, using wavelet analysis, the side view of metallic melt pools, and shows good agreement with the previously reported wave velocities and vibration frequencies. Finally, the presence of a keyhole during laser polishing is explored and shown to not be detrimental to surface smoothing and potentially beneficial for removing longer wavelength features.

* Corresponding author.
*E-mail address:* frank.pfefferkorn@wisc.edu (E. Pfefferkorn).

https://doi.org/10.1016/j.cirp.2019.04.110
0007-8506/

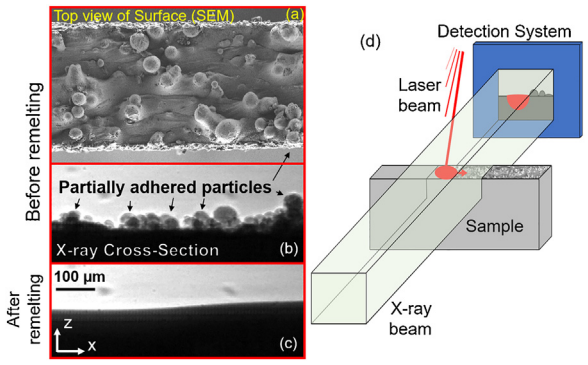


**Fig. 1.** The remelting process was observed using high-speed X-ray imaging (HSXRI). This figure shows the (a) SEM top view of the surface, (b) X-ray side view of the surface before remelting, and (c) X-ray side view following laser remelting. (d) Schematic of the experimental setup. The laser travels in the X-direction.

## 2. Experimental methods

### 2.1. Materials

The material used was a cobalt-chromium alloy (Celsit 21-P, Stellite 21 equiv.) that was manufactured using powder-bed fusion (SLM 250, SLM Solutions) with a nominal powder diameter distributed between 20 µm to 53 µm. All experiments were performed on the side of the additive-manufactured samples orthogonal to the build layer. The results in §3.3 were measured from regions laser remelted on bulk samples approximately 10 mm × 20 mm × 5 mm in size. The data presented in §3.1 and §3.2 from the HSXRI was on a sample nominally 10 mm × 0.32 mm × 5 mm cut out of the bulk material using electrical discharge machining. For the capillary wave dispersion relations, a density of 8350 kg/m$^3$ for Celsit 21-P [10] and a surface tension of 1.881 N/m for liquid cobalt at 1773 K [11] was used.

### 2.2. Laser remelting

The laser remelting performed in §3.1 and §3.2 for HSXRI used a 520 W max, 1070 nm fiber laser (IPG Photonics, IPG YLR-500-AC) operated in continuous wave (CW) mode with a Gaussian beam at a power of 200 W and directed by a laser scanner (SCANLAB, IntelliSCAN$_{de}$ 30). A 4 mm long line was scanned, of which the center 2 mm were observed using HSXRI. The laser used on the additional laser remelting experiments of §3.3 was a 200 W max, 1070 nm fiber laser (SPI Lasers, SP-200C-W-S6-A-B) also operated in CW mode with a Gaussian beam and directed by a laser scanner (SCANLAB, hurrySCAN II 14). The power was varied in these additional experiments. All experiments used a beam diameter of approximately 110 µm, a velocity of 200 mm/s, and Argon shielding gas at atmospheric pressure. The higher power conditions (>120 W) had a keyhole present, that can be seen in the X-ray imaging and can also be audibly detected.

### 2.3. High-Speed X-ray imaging

High-speed X-ray imaging (HSXRI) of the laser remelting process was performed at the Advanced Photon Source (APS), Argonne National Laboratory using the 32-ID-B beamline. The experiments used polychromatic X-rays with a first harmonic energy of 25 keV that was delivered using a short-period (1.8 cm) undulator with a 14 mm gap. The X-ray detector system include a 100 µm thick LuAG:Ce scintillator, a 45° reflection mirror, a relay lens, and an objective lens, and a high-speed camera (Photron, FASTCAM SA-Z). The captured images had a window size of 2.02 mm × 0.51 mm with a resolution of 1.974 µm/pixel. The recording was captured at 50 kHz with an exposure time of 1 µs per frame.

### 2.4. High-Speed X-ray image processing and wavelet analysis

The images captured from HSXRI were post-processed using computer software (MATLAB R2017b) to apply contrast adjustment. The edge of the melt pool was calculated by converting the image into a binary image using Otsu's method [12]. From the extracted top edge of the melt pool, the frequency of the surface height fluctuations was calculated using the continuous wavelet transform (CWT) with the Morlet wavelet and L1 normalization. The dispersion relationship between frequency and wavenumber of deep surface capillary waves can be described by Eq. (1) [13].

$$\omega^2 = \frac{\sigma}{\rho}|k|^3 \tag{1}$$

where $\omega$ is the angular frequency and $k$ is the wave number. This relationship, combined with Eqs. (2) and (3), relate the wavelength and frequency through Eq. (4):

$$\lambda = \frac{2\pi}{k} \tag{2}$$

$$\omega = 2\pi f \tag{3}$$

$$\lambda = \sqrt[3]{\frac{2\pi\sigma}{\rho f^2}} \tag{4}$$

where $\rho$ is the fluid density, $\sigma$ is the surface tension, $\lambda$ is the wavelength, and $f$ is the frequency.

### 2.5. Surface imaging and roughness analysis

The remelted surface studied with HSXRI was scanned beforehand using a focus variation optical microscope (Alicona InfiniteFocus G4) using a 20× objective with a vertical and horizontal resolution of 100 nm and 1.5 µm respectively. The roughness of the surfaces reported in §3.3 were imaged following laser remelting using the same technique, optic, and resolution. The waviness from the surfaces were filtered using a phase-corrected Gaussian filter, and the roughness values given are in accordance with ASME B46.1-2002 and ISO 25178 Areal -Part 2.

## 3. Experimental results and discussion

### 3.1. High-Speed X-ray imaging of remelting

The HSXRI captured various wave dynamic phenomena of the laser remelting process. Fig. 2 presents a representative melt period that reveals balling, particle incorporation, as well as wave formation, propagation, and decay. A specific point is highlighted by a blue dot in Fig. 2. The height of that specific point vs. time is shown in Fig. 3. Note that the group of images shown in Fig. 2 is part of a larger dataset covering more than a 6 ms timespan.

The height as the laser and the keyhole passes over it in Fig. 3 shows wave propagation inducing vibrations on the surface. The increase in steady-state height is the result of particle incorporation and surface tension causing the surface of the thin sample to partially round near the edges, and also reflects the thermal expansion of the sample caused by laser heating. The wavelet transform spectrogram of this signal is shown in Fig. 4a. The y-axis is presented in wavelength instead of frequency, which was transformed using Eq. 4. The spectrogram shows a strong vibration with a 300 µm wavelength. In addition to the dominant vibration at 300 µm, there are other vibrations that occur later in time due to waves propagating down the melt pool. As those waves propagate, they diffuse outwards causing an increased wavelength and decreased frequency. Fig. 4b is constructed by taking the maximum value at every wavelength and shows the maximum wavelength occurring around 300 µm. That same concept can then be applied to every point measured along the 2 mm sample and is shown in Fig. 4c. Fig. 4c shows that across the entire metal melt pool for the

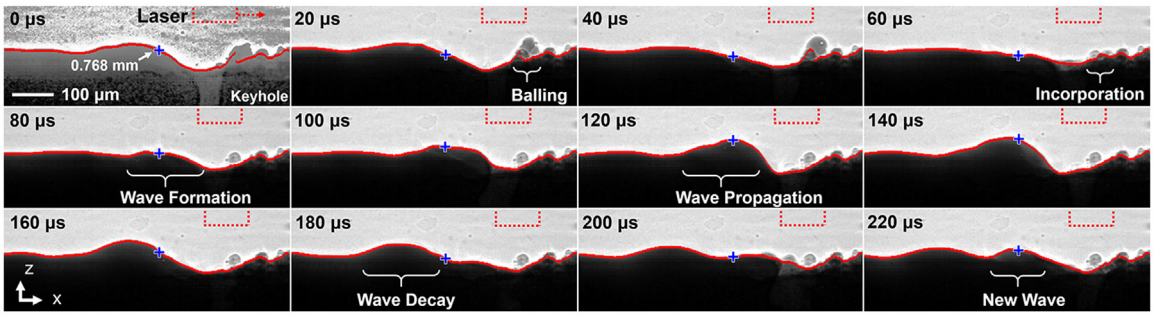


**Fig. 2.** Twelve frames captured from HSXRI. Several fluid phenomena, such as balling, particle incorporation, wave formation, wave propagation, and wave decay are highlighted. The red dashed box represents the approximate location of the laser. The 0 µs image has a modified contrast to better show the keyhole. The blue plus sign is a location analyzed in Figs. 3 and 4. The laser travels along the positive x-direction.

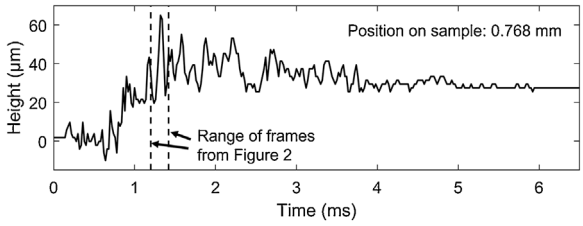


**Fig. 3.** The height of the specific point highlighted in Fig. 2 vs. time.

entire recording period the dominant wavelengths occur around 278 µm–441 µm, which correspond to frequencies between 4063 Hz–8125 Hz. Prior work has shown that a keyhole vibrates at similar values [8,9].

### 3.2. Features on the initial surface

The surface observed using HSXRI was measured prior to remelting, with an extracted 0.44 µm wide line of the surface shown in Fig. 5 and the corresponding 1D continuous wavelet transform of the line in Fig. 6. As these figures demonstrate, the surface contains a range of wavelengths due to the initial powder having diameters between 20 µm to 53 µm and from larger powder clusters on the surface that form during the build process.

Prior work on conduction mode laser polishing has proposed that the initial features are the features that are dampened during laser remelting according to their spatial frequency and a critical frequency that is related to the melt duration [14]. However, this work demonstrates the opposite for the keyhole mode– there is a dominate wavelength observed in the melt pool dynamics. Additionally, Fig. 2 shows the incorporation of a cluster of particles between 40 µs to 60 µs and the creation of a wave at 80 µs rather than a slower decay in the size of the particle as it incorporates. This implies that the frequencies observed are due to the keyhole inducing specific vibrations into the melt pool.

### 3.3. Effect of laser remelting on surface roughness

The surface roughness following laser remelting was also measured for a range of laser powers and is shown in Fig. 7.

There are three approximate continuous wave laser polishing modes that are highlighted in the figure: insufficient melting, where the laser has too low of power, conduction mode polishing, where the vapor depression is absent, and keyhole mode where a keyhole has formed. The surface roughness in these plots can be modeled using the following exponential model:

$$S_a(\lambda) = S_{a,primary}\left[1 - \exp\left(-\frac{\lambda}{\lambda_{crit}}\right)\right] \quad (5)$$

where $S_a$ is the surface roughness as a function of cutoff wavelength, $S_{a,primary}$ is the surface roughness without any waviness filter, $\lambda$ is the cutoff wavelength, and $\lambda_{crit}$ is a critical

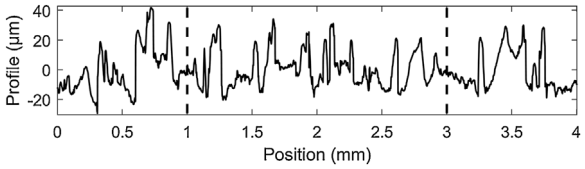


**Fig. 5.** Height of the surface before laser remelting. The dashed lines represent the approximate range which the HSXRI captured.

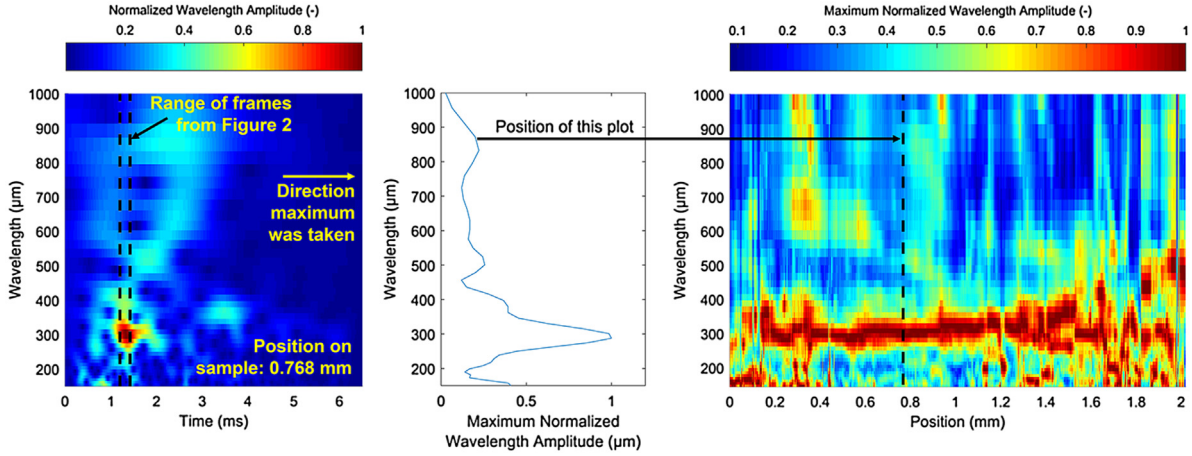


**Fig. 4.** Using the CWT to analyze surface fluctuation of the melt pool. (a) This shows the CWT spectrogram of the surface from Fig. 3 and (b) the maximum value for every wavelength of Fig. 4a. (c) Shows wavelengths measured when the Fig. 4b process is applied to every point in the surface. The dominate vibration wavelength for most positions occur between 300 µm to 400 µm.

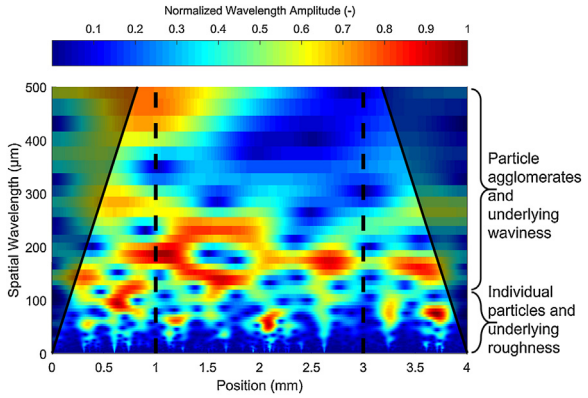


**Fig. 6.** The CWT spectrogram of the surface prior to laser remelting shows it contains a range of wavelengths. The shaded region represents the cone of influence where edge effects reduce the accuracy of the CWT, and the dashed lines show the HSXRI region.

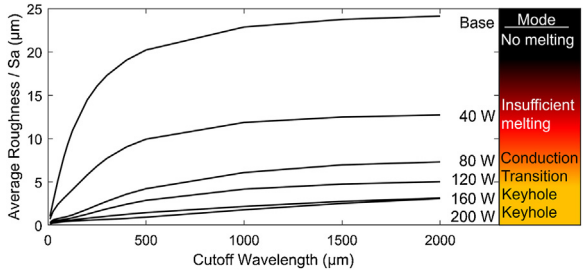


**Fig. 7.** Surface roughness ($S_a$) vs. cutoff wavelength for a range of laser powers. The base – 160 W represents the mean value of 4 areas, while the 200 W condition was measured from the surface remelted in §3.2.

wavelength that represents the wavelength above which 36.8% of the roughness remains. These values are given in Table 1.

As Table 1 demonstrates, the critical wavelength grows larger with increasing power and the formation of a keyhole. A higher critical wavelength implies there has been more effective reduction of the wavelengths below it. This indicates that a keyhole should not necessarily be avoided, and for very rough starting surfaces may help achieve a lower roughness that would not be possible without it. Additionally, the higher laser absorption and corresponding larger melt pool and melt depth caused by the keyhole may also aid in polishing highly reflective metals such as aluminum, copper, and magnesium. However, there are other considerations when a keyhole is present, such as keyhole induced porosity, hot cracking, and more that users must consider.

## 4. Conclusions

This work presents the first example showing high-speed X-ray imaging (HSXRI) of laser remelting with the objective of surface smoothing and polishing. It also presents the analysis of metallic fluid waves using wavelet analysis, and provides valuable data on dominant melt pool frequencies and wavelengths for future modeling work. It informs that modeling of feature incorporation during laser remelting using the initial surface features does not hold at certain lasing conditions, and encourages the development of new models that can capture these phenomena of surface waves induced by keyhole mode laser melting. Additionally, the HSXRI demonstrates that particles predominately get incorporated into the surface rather than ejected during laser remelting, even in the presence of a keyhole, and shows particles balling together prior to incorporation.

This work also informs that a keyhole is not necessarily detrimental for laser polishing, and can aid in removing longer wavelength features due to enabling a longer and deeper melt pool. However, laser polishing a relatively smooth initial surface in keyhole mode may cause an increase in surface roughness due to large wavelength features created by the surface waves. Additionally, keyhole mode laser melting can cause porosity and solidification cracking that could potentially reduce mechanical properties. However, there is active research on methods for preventing keyhole collapse during laser welding that could help reduce and eliminate keyhole porosity [4,5], which could make continuous wave laser polishing with a keyhole a beneficial first step for smoothing high starting roughness parts.

**Table 1**
Roughness values and critical wavelength.

| Power (W) | 200 | 160 | 120 | 80 | 40 | Base |
|---|---|---|---|---|---|---|
| $S_{a,primary}$ (μm) | 5.8 | 3.9 | 5.5 | 7.7 | 13.1 | 24.8 |
| $\lambda_{crit}$ (μm) | 2578 | 1072 | 696 | 654 | 335 | 240 |
| Adjusted $R^2$ | 0.973 | 0.964 | 0.995 | 0.995 | 0.993 | 0.988 |

## Acknowledgements

This work was supported by National Science Foundation (NSF) grant CMMI-1727366, NSF-supported shared facilities at UW-Madison, and Deutsche Forschungsgemeinschaft grant 386371584. This research used resources of the Advanced Photon Source, a U.S. Department of Energy (DOE) Office of Science User Facility operated for the DOE Office of Science by Argonne National Laboratory under Contract No. DE-AC02-06CH11357. The authors thank Cang Zhao, Alex Deriy, and Kamel Fezzaa for their assistance with the beamline experiment.

## Appendix A. Supplementary data

Supplementary material related to this article can be found, in the online version, at doi:https://doi.org/10.1016/j.cirp.2019.04.110.

## References

[1] Schmidt M, Merklein M, Bourell D, Dimitrov D, Hausotte T, Wegener K, Overmeyer L, Vollertsen F, Levy GN (2017) Laser Based Additive Manufacturing in Industry and Academia. *CIRP Annals – Manufacturing Technology* 66/2:561–583.
[2] Brinksmeier E, Riemer O, Gessenharter A, Autschbach L (2004) Polishing of Structured Molds. *CIRP Annals — Manufacturing Technology* 53/1:247–250.
[3] Bordatchev EV, Hafiz AMK, Tutunea-Fatan OR (2014) Performance of laser polishing in finishing of metallic surfaces. *The International Journal of Advanced Manufacturing Technology* 73:35–52.
[4] Schmidt M, Zäh M, Li L, Duflou J, Overmeyer L, Vollertsen F (2018) Advances in macro-scale laser processing. *CIRP Annals – Manufacturing Technology* 67/2:719–742.
[5] Katayama S, Mizutani M, Matsunawa A (2003) Development of Porosity Prevention Procedures During Laser Welding. *First International Symposium on High-Power Laser Macroprocessing*, 4831.
[6] Zhao C, Fezzaa K, Cunningham RW, Wen H, De Carlo F, Chen L, Rollett AD, Sun T (2017) Real-time Monitoring of Laser Powder Bed Fusion Process using High-speed X-ray Imaging and Diffraction. *Scientific Reports* 7/1:3602.
[7] Parab ND, Zhao C, Cunningham R, Escano LI, Fezzaa K, Everhart W, Rollett AD, Chen L, Sun T (2018) Ultrafast X-ray Imaging of Laser-melt Additive Manufacturing Processes. *Journal of Synchrotron Radiation* 25/5:1467–1477.
[8] Pang S, Chen L, Zhou J, Yin Y, Chen T (2011) A Three-dimensional Sharp Interface Model for Self-consistent Keyhole and Weld Pool Dynamics in Deep Penetration Laser Welding. *Journal of Physics D: Applied Physics* 44. 025301.
[9] Ki H, Mohanty PS, Mazumder J (2002) Modeling of Laser Keyhole Welding: Part II. Simulation of Keyhole Evolution, Velocity, Temperature Profile, and Experimental Verification. *Metallurgical and Materials Transactions A* 33/6:1831–1842.
[10] Böhler Welding, Metal Powder and Continuous Casting Rods, 26, http://www.bohlerwelding.ru/files/cat/metallpulver.pdf, 18-Dec-2018.
[11] Keene BJ (1993) Review of Data for the Surface Tension of Pure Metals. *International Materials Review* 38/4:157–192.
[12] Otsu N (1979) A Threshold Selection Method from Gray-level Histograms. *IEEE Transactions on Systems Man and Cybernetics* 9/1:62–66.
[13] Landau LD, Lifshitz EM (1987) Course of Theoretical Physics... *Fluid mechanics*, 2nd edition, vol. 6 244–245. Oxford.
[14] Vadali M, Ma C, Duffie NA, Li X, Pfefferkorn FE (2012) Pulsed Laser Micro Polishing: Sutpdelrface Prediction Model. *Journal of Manufacturing Processes* 14/3:307–315.